Collective Atomic Recoil Lasing and Superradiant Rayleigh Scattering in a high-Q ring cavity

Sebastian Slama, Gordon Krenz, Simone Bux, Claus Zimmermann and Philippe W. Courteille

Physikalisches Institut, Eberhard-Karls-Universität Tübingen, Auf der Morgenstelle 14, D-72076 Tübingen, Germany

Abstract. Cold atoms in optical high-Q cavities are an ideal model system for long-range interacting particles. The position of two arbitrary atoms is, independent on their distance, coupled by the back-scattering of photons within the cavity. This mutual coupling can lead to collective instability and self-organization of a cloud of cold atoms interacting with the cavity fields. This phenomenon (CARL, i.e. Collective Atomic Recoil Lasing) has been discussed theoretically for years, but was observed only recently in our lab. The CARL-effect is closely linked to superradiant Rayleigh scattering, which has been intensely studied with Bose-Einstein condensates in free space. By adding a resonator the coherence time of the system, in which the instability occurs, can be strongly enhanced. This enables us to observe cavity-enhanced superradiance with both Bose-Einstein condensates and thermal clouds and allows us to close the discussion about the role of quantum statistics in superradiant scattering.

INTRODUCTION

An astonishing phenomenon is reported from populations of fireflies [1]. Individual fireflies are emitting light in a randomly flashing way. However, if the population exceeds a certain number of individuals, the uncorrelated flashing of the single flies synchronizes such that a large part of the population flashes in phase with each other and 'seems to agree' on a common flashing frequency. This principle of self-synchronization can be found in many other biological, social, chemical and physical systems, as for example in the frequency-locking of laser arrays or in the walking behavior of people on bridges [2, 3]. All of these systems can be described in a very general model, the Kuramoto model, which is based on a collection of weakly coupled oscillators [4].

The same model applies to clouds of cold atoms, if the individual atoms experience an interaction. Such an interaction can for example be generated by the scattering of photons. If the interaction is weak, atoms scatters photons individually and are not influenced by the scattering of other atoms. This is even true for Bose-Einstein condensates (BEC), where all atoms are delocalized over the same region of space. If the atoms do not show long-range order, such individual scattering manifests in a scattered light intensity which is proportional to the number of scatterers. In contrast, if the interaction is strong enough, the individual scattering events can be synchronized such that all atoms contribute in a cooperative way. Scattering then evolves as

a global dynamics of the whole cloud, with the scattered intensity being enhanced by the phase coherent emission of light fields and depending on the number of scatterers with a power law larger than one. A prominent example for this behavior is Dicke superradiance [5]: a dense cloud of electronically excited atoms synchronizes its spontaneous emission and emits a light pulse with an intensity which depends quadratically on the number of atoms. However, we must bear in mind that similar dependencies can also arise due to an externally imposed long-range order of the cloud rather than to self-synchronization. This is for example true for Bragg-scattering from atomic clouds which are periodically arranged by means of an optical lattice [6, 7, 8, 9]. Interestingly, long-range order can arise due to the self-synchronization process itself. In this case we talk about self-organization of structures. Again there is a tremendous amount of examples of self-organizing real systems of which just one is the formation of natural landform patterns such as meandering rivers or sand dunes [10].

In this paper we are dealing with two types of experiments with ultracold atoms, which are coupled by the scattering of photons, namely superradiant Rayleigh Scattering (SRyS) on one hand [11, 12] and Collective Atomic Recoil Lasing (CARL) on the other [13, 14]. Both experiments show self-organization leading to the spontaneous formation of a density grating of atoms. We will present our measurements of CARL in different regimes by which we will show that the two experiments are instrinsically connected with each other.

CARL AND SRYS

CARL has been proposed for atomic gases which are illuminated by a strong optical pump field [15, 16]. The atoms scatter photons from the pump field into an unpumped probe field. The acceleration due to photonic recoil, experienced by the atoms, depends on the atomic position in such a way that the atoms are arranged in a density grating, which fulfills the Bragg condition and in turn enhances the scattering. This effect is particularly strong, if pump- and probe light fields are modes of an optical high-Q ring cavity and, up to now, has only been observable in cavities.

SRyS on the other hand has been observed in free space. The atoms scatter light from a short pump pulse into a probe light field and are accelerated in units of the recoil momentum $p_r = 2\hbar k$, with k the wavevector. This leads to the occupation of different momentum states, which by matter-wave interference build up a density grating and in turn enhance the scattering. Due to the fact that, at the beginning, SRyS could only be observed with BECs, and although in 2005 superradiant Raman scattering was observed with atoms slightly hotter than the critical temperature for Bose-Einstein condensation [17], some discussions about the role of quantum statistics and the importance of Bose-enhancement for SRyS arose[18, 19]. From our present point of view, the prediction that the relevant phenomenon for SRyS is not the quantum state of the atoms but their cooperative behavior [11], was already confirmed by the first observation of CARL [20] with 100 μK cold atoms, which is two orders of magnitude hotter than

the condensation temperature. But it took us until now when we observed CARL in a regime with superradiance-like dynamics and directly measured the dependence on the temperature, that we fully understood the connection between CARL and SRyS and could generalize our former results to superradiance.

What CARL and SRyS have in common is the gain mechanism [21], which in both cases is based on a positive feedback between a probe light field and an atomic density grating. The gain, which is given by the growth rate of the probe light field, depends on the frequency of the light field $G(\omega)$ and has a certain gain bandwidth $\delta\omega_G$. The analogy shows even up as formal identity of the gain in both cases [22, 23, 24]. Due to this formal concordance we might wonder, why CARL works with rather hot thermal atoms, while SRyS is restricted to the ultracold regime. The answer lies in the fact that the self-amplification works only within the coherence time of the system. The difference between the effects is, how the coherence of the system is preserved. In the case of SRyS the coherence time is given by the stability of the relative phase between different atomic matter waves. If the relative phase is smeared out, the density grating vanishes and the superradiant emission of light is stopped. For this reason SRyS is very sensitive to temperature effects, because a defined phase can only be attributed to the matter waves if the atomic Doppler broadening is much smaller than the momentum imparted by a single photonic recoil. In the case of CARL the situation is changed by the presence of the cavity, which leads to a very long life-time of both the pump- and the probe light field on the order of several μs, which is given by the cavity linewidth κ_C. The coherence can thus be preserved as the relative phase of the cavity light-fields, which is independent of the atomic motion. The atoms are then forced to maintain in the density grating by the optical lattice in the cavity, even if they are rather hot. Temperature effects on CARL do exist and we examine those within this paper, but these are much less dramatic than in the experiments dealing with SRyS.

CARL IN VARIOUS REGIMES

CARL may occur in four different regimes with each of them showing a characteristic dynamics of the atoms (Fig.1). Until now, all CARL-experiments [20, 25] had been performed in the good cavity regimes, whereas all experiments dealing with SRyS [11, 12, 17] had taken place very far in the bad-cavity regimes. In our latest experiments [13, 14] we have been able to examine the transition between these regimes by changing the finesse of the cavity. What discerns the good cavity from the bad cavity regime is the size of the cavity linewidth compared with the recoil frequency $\omega_r = p_r^2/2m\hbar$. The linewidth determines the density of states inside the cavity and limits the range of frequencies accessible for the probe light field. The frequency of the scattered photons is on the other hand Doppler shifted with respect to the pump light frequency, which we lock to a cavity resonance. The size of the shift is given by the momentum of the scattering atoms. For that reason a cavity linewidth which is smaller than the recoil frequency (which is the distance between neighboring momentum states in frequency space), like shown in Fig. 1 (a) and (c), limits the atomic dynamics to the momentum
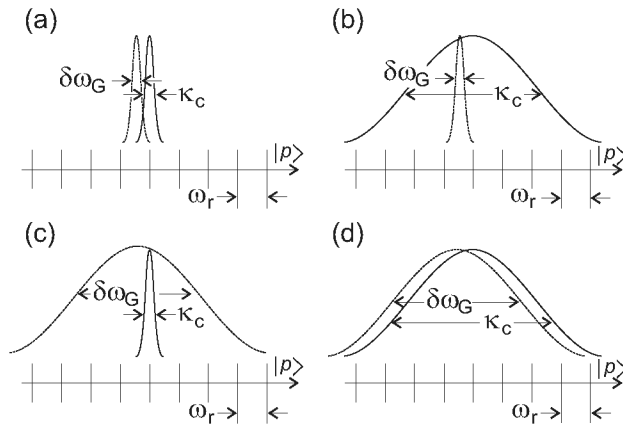
321

FIGURE 1. Schematic illustration of the four CARL regimes. (a) Quantum good-cavity regime, (b) quantum bad-cavity regime, (c) semiclassical good-cavity regime and (d) semiclassical bad-cavity regime.

state $|p\rangle = |0\rangle$ and its closest neighbors. This case is called the good cavity regime. If on the other hand, like in Fig. 1 (b) and (d), the cavity linewidth is larger than the recoil frequency, all momentum states which are lying within the linewidth may participate in the CARL dynamics. In that sense the difference between good and bad cavity is the principle frame, in which the dynamics may take place. But how the dynamics takes place within this frame is determined by yet another variable, namely the gain bandwidth $\delta\omega_G$. The ratio between the gain bandwidth and the recoil frequency determines, how many momentum states are amplified at the same time. If for example the ratio is smaller than one, Fig. 1 (a) and (b), which is called the quantum regime, only two neighboring momentum states are coupled with each other. This leads to a coherent behavior like in a two level system, such that at any time the momentum population is distributed to a maximum value of just two momentum states. If one the other hand the ratio between the gain bandwidth and the recoil frequency is larger than one, Fig. 1 (c) and (d), which is called the semiclassical regime, several momentum states are coupled at a time. In this case the initial momentum distribution, even if only one momentum state was occupied like in a BEC, is spread over several momentum states by the dynamics. The occupation of more and more momentum states then leads to a decreasing bunching of the atoms and consequently to decoherence of the system. [1]

---

[1] While discerning between good cavity, bad cavity, quantum and semiclassical regime, we have to bear in mind, that the explained distinction by cavity linewidth and gain bandwidth is useful for understanding the underlying physics, but the quantities delimiting the regimes have a complicated interdependence. It is for example possible, that the dynamics would be, according to the cavity linewidth, in the good cavity regime. Nevertheless a very large gain bandwidth may broaden the spectrum of excited momentum states as in the bad cavity regime. A thorough description resorts to dimensionless, independent parameters, which are called CARL parameter ρ and scaled linewidth κ [22].

322

EQUATIONS OF MOTION

Our system consists of ultracold atoms and Bose-Einstein condensates interacting with the counterpropagating modes of a high-Q ring cavity. For a general approach which describes mean field interactions or quantum statistical effects such as nonlocal particle correlations, particle fluctuations or entanglement, both the light and the matter wave modes would have to be treated as quantized [26, 27]. However, in the case of our experiments, several simplifications can be made:

(1) The detuning of the pump laser frequency to the closest atomic resonance is on the order of several THz, such that the population of all electronically excited states is negligible. These states can then by adiabatically eliminated [16]. (2) For the same reason the optical density of the atomic cloud is so low, that propagation effects of light inside the cloud need not to be considered [28]. (3) In the semiclassical regime, where our experiments take place, quantum effects, such as entanglement which may occur in CARL [27], are negligibly small. (4) We are working with high laser powers, such that the light fields can be treated classically. (5) We are describing the dynamics of our system only along the cavity axis, i.e. in one dimension. Transversal effects in CARL exist [29], but are not considered, because they are much weaker than the axial dynamics. (6) The backaction of the atoms on the pump light field is neglected, because typical probe light powers are three orders of magnitude weaker than the pump light power, which allows us to make a nondepleted pump approximation. Experimentally the pump laser frequency is phase-locked to a resonance of the cavity, such that there is a fixed phase-relation between the pump laser field and the intracavity pump mode field amplitude α_+. The lock compensates also for the shift of the cavity resonance due to the change of the refractive index when atoms are loaded into the cavity. We keep our system in the regime of weak coupling between the cavity modes and the atoms, where splitting of the cavity resonance into two normal modes, which was observed in [30], is negligible. For these reasons the phase of the pump mode field can be chosen arbitrarily, which we do by setting α_+ real. Within these approximations our system is well described by the equations

$$
\begin{aligned}
\frac{dp_j}{dt} &= -2i\hbar k U_0 \alpha_+ \left(\alpha_-^* e^{2ikz_j} - \alpha_- e^{-2ikz_j} \right) , \\
\frac{d\alpha_-}{dt} &= -(\kappa_c + i\Delta_c)\alpha_- - iU_0\alpha_+ \sum_{j=1}^{N} e^{-2ikz_j} .
\end{aligned}
\tag{1}
$$

These equations describe the dynamics of N atoms with momenta p_j and positions z_j and of the probe light field α_-. The force acting on the atoms is the dipole force, which is proportional to the single photon light shift U_0. The left term in the lower equation for the probe light field contains losses with the cavity linewidth κ_c and phase shifts which are proportional to the detuning from the cavity Δ_c (in our case is $\Delta_c = 0$). The right term represents the scattering of photons from the pump mode into the probe mode and is proportional to the bunching of the atoms, which is given by $b = N^{-1}\sum_j e^{-2ikz_j}$. Radiation pressure and light scattering from the mirror surfaces lead to observable
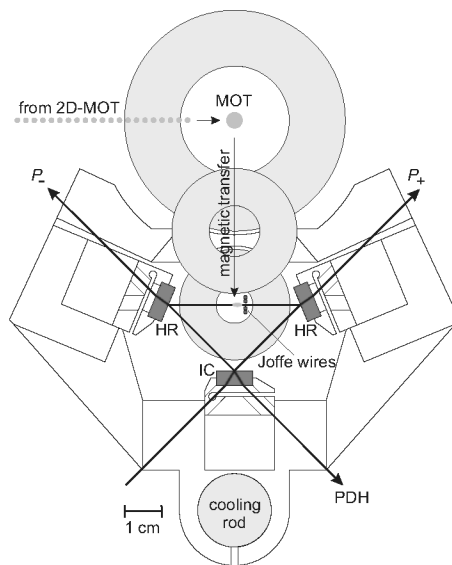
FIGURE 2. Technical drawing of our setup.

perturbations in our experiments and can also be included into the equations, as shown in [14].

EXPERIMENTAL PROCEDURE AND MEASUREMENTS

Our setup shown in Fig. 2 combines the techniques to produce Bose-Einstein condensates with a high-Q high ring cavity. All parts including magnetic coils, wires and the cavity are located inside a vacuum chamber. A cold atomic beam of ^{87}Rb is produced by a two-dimensional magneto-optical trap (2D-MOT) within a second vacuum chamber and is directed into the main chamber, where it is recaptured in a standard MOT. From there the atoms are loaded into a magnetic trap, which is formed by the same quadrupole coils as the MOT. Then, the atoms are transferred magnetically via a second into a 5 cm distant third pair of coils and are thereby adiabatically compressed. The compressed atoms are loaded into a Joffe-Pritchard type of wire trap produced by the coils and four vertically directed wires, where they are cooled by forced evaporation with a microwave frequency. Typical oscillation frequencies in this harmonic trap are $\omega_r = 200$ Hz and $\omega_z = 50$ Hz at a magnetic offset field of $B_0 = 2$ G with the longitudinal z-direction pointing along the cavity axis. We can produce Bose-Einstein condensates with typically several 10^5 atoms. For most of the experiments reported in this paper however, we have been using ultracold thermal clouds, because quantum degeneracy is unnecessary for CARL. After the evaporation the atoms are transferred vertically about 1 mm into the mode volume of the cavity. The cavity consists of one plane (IC) and two curved (HR) mirrors with a curvature of $R_c = 10$ cm. The round-trip length of the
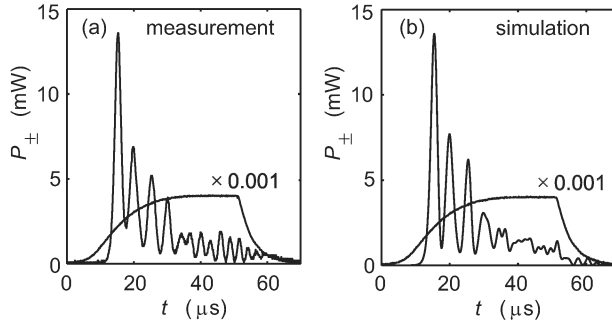
324

FIGURE 3. (a) Typical measured time curves of pump and probe light power. In this measurement the experimental parameters are $N = 1.5 \times 10^6$, $P_+ = 4$ W, $\lambda = 797.3$ nm, and $F = 87000$. For visibility the pump-light power is scaled down by a factor of 0.001. (b) Simulation of the CARL-equations. We used the measured rise of the pump-light power within the simulation and fitted the experimental parameters in order to agree with the measurement. The fitted parameters are in reasonable agreement with the measured ones.

cavity is 8.5 cm, corresponding to a free spectral range of $\delta_{fsr} = 3.5$ GHz. The finesse of the cavity depends on the polarization of light and adopts values of $F = 87000$ for p-polarization and $F = 6500$ for s-polarization.

As soon as the atoms are positioned inside the cavity, we switch on the pump light, which is fed into the cavity via the IC mirror. The light reflected from the mirror is used to Pound-Drever-Hall (PDH) stabilize the light frequency to the cavity resonance. Due to the finite bandwidth of the locking servo is takes approximately $20\ \mu$s until the pump light field in the cavity has built. After a time of $t = 50\ \mu$s we switch off the pump light field. In the mean time the CARL dynamics is starting and a train of probe light pulses like shown in Fig. 3 is emitted. This characteristic behavior can be most easily explained within the quantum regime, where the atomic momenta are distributed only between neighboring states. If all atoms are in the same momentum state, like in a BEC, light scattering is suppressed, because the position distribution of a single momentum state is homogeneous. When however, due to CARL, more and more atoms are brought into the neighboring momentum state, matter-wave interference leads to an increasingly developed density grating of atoms, which enhances the scattering. The maximum contrast of the grating is reached, when the two neighboring momentum states are equally populated. This is the point, when also the probe light power reaches its maximum. The further dynamics again concentrates the population in one of the two momentum states, and the density grating and hence the probe light are vanishing. This dynamics repeats in a self-similar way, until decoherence smears out the dynamics. This can be seen in Fig. 3 as decrease of the envelope of the train of pulses and is due to the increasing spread of the occupied momentum states in the semiclassical regime. In the following chapters we will examine the dependence of the probe light power on certain experimental parameters. In particular we analyze the power at the first maximum $P_{-,1}$ and the time interval between the first and the second maximum $\Delta t_{1,2}$, which is the typical timescale, in which the momentum changes by one recoil $p_r = 2\hbar k$. The parameters we are changing are the
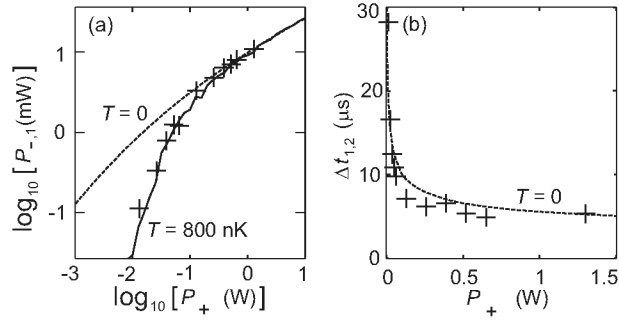
325

FIGURE 4. Dependence of (a) the peak probe power P_{-1} and (b) the time delay between the first two peaks $\Delta t_{1,2}$ on the pump power P_+. Simulations are done without free parameters. Residual fluctuations in the simulation for $T = 800$ nK are due to the statistics occuring for a limited simulated atom number of $N_S = 100$. The experimental parameters are $N = 2.4 \times 10^6$, $\lambda = 796.1$ nm, and $F = 87000$. The stochastic error of the measurements is smaller than the marker size.

atom number N, the intracavity pump light power P_+, the finesse of the cavity F and the atomic temperature T. Dependences on perturbations such as mirror backscattering are reported in [14]. Simulation results which we compare with our measurements are obtained by numerical integration of Eq. (1) with the explicit Euler method, calculating the trajectories of $N_S = 100$ atoms, each representing N/N_S real atoms.

Pump power

The pump light power influences the dynamics of the collective instability. If the pump power is reduced, also the contrast of the optical standing wave decreases, which is formed by interference between pump and probe light field. This weakens the collective dynamics and leads to a reduced probe light power. In previous experiments, where we exposed cold atoms inside a high-Q ring cavity to the dissipative and diffusive forces of an optical molasses, we observed a threshold behavior of the pump power [25]. Only if the pump power was above threshold, the CARL dynamics could be observed. In the present setup the atoms are not exposed to a strong dissipative reservoir, such that it is not fully clear, whether or not CARL with Bose-Einstein condensates involves a threshold. The only channel to dissipation in the present setup is the transmission through the cavity mirrors, which is on the order of few ppm. By that the cavity modes are coupled to the electromagnetic field of the surroundings, which at room temperature is in a very good approximation a zero-temperature reservoir of photons. The interaction with this reservoir is therefore only dissipative, but not diffusive. On the other hand Bose-Einstein-condensates are object to quantum fluctuations. It is an open question, whether such fluctuations can lead to a threshold behavior.

In the measurements shown in Fig. 4 the pump power could for technical reasons only be reduced to values of $P_{+,\text{min}} \approx 10^{-2}$ W inside the cavity. Within this accessible

range, we observed that temperature effects can lead to a strong threshold-like reduction of the probe light power. The data agree very well with simulations (solid line) using the experimentally measured parameters and a temperature of the atoms of $T = 800$ nK. The dotted line is a simulation with the same parameters, but with a temperature of $T = 0$. Above a pump power of about $P_+ = 0.1$ W, both curves coincide. Below this value the probe light power decreases much faster for a finite temperature of the atoms. This behavior can be explained by the fact, that depending on the temperature of the atoms the initial momenta are spread over a number of momentum states given by the Doppler width. However, only those atoms can participate in the CARL dynamics, whose momenta are within the gain bandwidth, which depends on the pump power. If by reduction of the pump power the gain bandwidth gets smaller than the Doppler width, the effective number of atoms for CARL is reduced. This leads to the observed decrease of the probe light power. Another interesting observable is the time difference $\Delta t_{1,2}$ between successive maxima in the probe light power, because is represents the typical time scale in which the momentum population is shuffled between neighboring momentum states. The larger the gain is, the faster is this time scale. This behavior can be seen in Fig. 4 (b), where our measurements agree well with a simulation with the above given parameters and a temperature of $T = 0$. At finite temperature and small pump powers a slight reduction of the time difference is observed, however this correction is very small, such that for visibility we do not plot the simulation with $T = 800$ nK.

Finesse and atom number

As explained above, the CARL model includes different regimes, which are known as good-cavity and bad-cavity regime. With our experiment we could for the first time explore both regimes by changing the finesse of the cavity. Which regime is reached can be analyzed from the way the probe light depends on the experimental parameters. In the good-cavity regime, which is typical for CARL, the maximum probe power scales like $P_{-,1} \propto N^{4/3} P_+^{1/3}$, whereas in the bad-cavity regime the scaling is like $P_{-,1} \propto N^2 P_+$, which is typical for superradiance. It is clear that at some point there must be a transition from the one to the other behavior. This transition however is not a sudden change, but rather a gradual crossover. The above given scalings are reached in the limiting cases of a very good and very bad cavity.

In order to determine the dominating regimes in our measurements, we have been analyzing the dependence on atom number. The results for two different values of the finesse are shown in Fig. 5. We compare our measurements with both limiting scalings (dotted and dashed lines) and show simulations of the CARL equations (solid lines) for the experimental parameters. The simulations confirm that, although our measurements are still close to the interface of both regimes, the expected behavior for $F = 87000$ (high finesse) is clearly CARL-like, whereas for $F = 6400$ (low finesse) it is clearly superradiance-like. In fact our measurements show the expected behavior, i.e. for high finesse we observe a scaling of the maximum probe power typical for the good-cavity regime, whereas for low finesse it approximates the bad-cavity behavior for large atom numbers. For low atom numbers the CARL-dynamics is suppressed by mirror backscat-
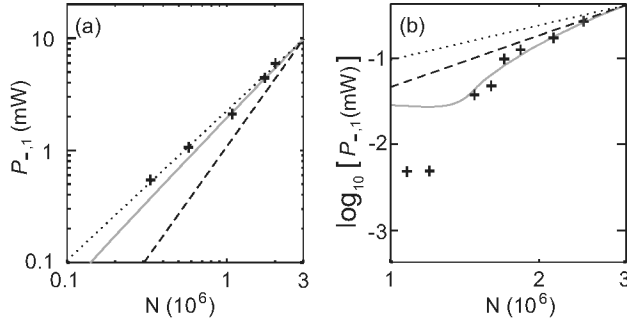
FIGURE 5. Measured dependency of the maximum probe light power on the atom number for two different values of the finesse. The experimental parameters are (a) $P_+ = 1.4$ W, $\lambda = 796.1$ nm, $F = 87000$ and (b) $P_+ = 66$ mW, $\lambda = 795.4$ nm, $F = 6400$. By comparison of the data points with the asymptotic behavior shown by the dotted and dashed lines, (a) can be identified as good-cavity regime and (b) as bad-cavity regime. The behavior is confirmed by measurements without free parameters (solid lines). The values of the data points are scaled by (a) 0.75 and (b) 2.8 in order to improve agreement with the simulations. We justify this multiplication by systematic errors which occur due to uncertainties in the calibration of the probe light power. Because the calibration depends on the polarization of probe light field, we assume a different scaling for low and good finesse. We emphasize that the relevant value, i.e. the dependency on the atom number, which is given by the slope in the logarithmic plot, is not changed by this pure multiplication.

tering, which can also be seen in the simulation, where this perturbation was taken into account. This effect is discussed in [14, 24].

Temperature

With our setup we can vary the temperature of the atoms in a range from $T < 1$ μK to several tens of μK. This allows us to systematically investigate the influence of the atomic temperature on the CARL dynamics and identify the role of quantum statistical effects ocurring with Bose-Einstein condensed clouds. Figure 6 (a) shows recorded time signals of the probe light power for thermal atoms with different temperatures. The corresponding curves are vertically shifted for clarity. We observe a decrease of the maximum probe power with increasing temperature.[2] The reason is again, that the increasing Doppler width of the atomic momentum distribution gets larger than the gain bandwidth, which in this experiment had been kept constant. This leads to a decreasing effective number of atoms participating in the CARL dynamics. This also explains, why in Fig. 6 (a) CARL is not observable at a temperature of $T = 40$ μK, while in our former experiments [20, 25] CARL was observed even with 100 μK hot atoms. The reason lies in the difference of the atom number of now $N = 10^6$ to formerly $N = 10^7$. A larger atom number increases the gain bandwidth, which in turn increases

---

[2] The bottom curve in Fig. 6 shows no feature of CARL, but the signal is due to mirror backscattering.
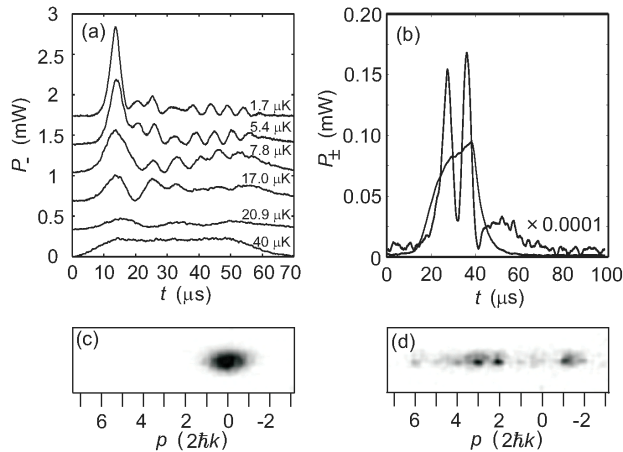
328

FIGURE 6. (a) Measured time signal of the probe light power for different atomic temperatures. For clarity the curves are shifted by 0.35 mW from each other. Throughout all measurements the experimental parameters were held constant at $N = 10^6$, $P_+ = 0.7$ W, $\lambda = 796.1$ nm, $F = 87000$. (b) Time signal of pump and probe light power during the CARL dynamics of a Bose-Einstein condensed cloud with experimental parameters $N \approx 10^5$, $P_+ = 0.7$ W, $\lambda = 796.1$ nm, $F = 87000$. The pump power is scaled down by a factor of 10^{-4} for clarity. The respective momentum distribution is shown in the time of flight pictures (c) before and (d) after the CARL dynamics, which have been recorded after 10 ms of adiabatic expansion.

the possible Doppler width where CARL is observable. The important point in Fig. 6 (a) is the fact that we do observe CARL at temperatures which are far above the critical temperature for Bose-Einstein condensation, which is below one μK. This proves clearly that quantum statistical effects are not important for the occurrence of both CARL and SRyS, which, as shown above, are based on the same physical phenomenon. Nevertheless it is interesting to see, what happens, when CARL is done with a condensed cloud of atoms. This is illustrated in Fig. 6 (b), which shows the measured time signals of pump and probe power. The probe light power cannot be directly compared with the one in Fig. 6 (a), because the atom number in (b) is on the order of $N = 10^5$ compared to $N = 10^6$ in (a). The signal is for this reason weaker in the case of a BEC. Apart from that quantitative difference, however, we do not observe a qualitative change of the behavior. This is also illustrated in Fig. 6 (c) and (d), which show the momentum distribution corresponding to Fig. (b) in time of flight pictures before and after the CARL dynamics. We observe that, as expected for a BEC, initially a single momentum state is occupied, whereas CARL leads to the population of several momentum states. This broadening is typical for the semiclassical regime and is equivalent to the observation of momentum spread in [31].

CONCLUSION

The topic of our experiments presented in this paper is the collective behavior of atoms inside a high-Q ring cavity, which is known as CARL and leads to the self-organization of the atoms into a periodic density grating. We have been able to measure CARL with ultracold thermal and Bose-Einstein condensed atoms, at the same time providing the first experimental realization of a BEC inside an optical cavity. With this setup we could observe CARL in two different regimes, which are known as bad-cavity and as good-cavity regime [21]. In these regimes the dynamics is superradiance-like resp. CARL-like. The observed characteristics of the instability allowed us to clearly identify the two regimes and show the intrinsic connection between CARL and superradiant Rayleigh scattering [11]. By our former observation of CARL with $T \approx 100 \ \mu$K cold atoms and by our new detailed analysis of CARL as a function of the temperature between values of $T \approx 1 \ \mu$K and $T \approx 40 \ \mu$K we proved experimentally that CARL and hence also SRyS do not require a quantum degeneracy of the atoms, but rely only on the cooperative behavior of the atoms [19].

Although the quantum statistics of the atoms does not play a role in our present experiments in future experiments it will be interesting to extend our studies to the quantum regime, where the dynamics is completely coherent. Within this regime photonic and matter-waves may be coherently coupled during the CARL dynamics. This may lead to the generation of entangled states between atoms and photons [27].

ACKNOWLEDGMENTS

REFERENCES

1. J. Buck, E. Buck, *Nature* News **211**, 562 (1966).
2. S. H. Strogatz, *Nature* (London),**410**, 268 (2001).
3. S. H. Strogatz et al., *Nature* (London), **438**, 43 (2005).
4. Y. Kuramoto, *Prog. Theor. Phys. Suppl.*, **79**, 223 (1984).
5. R. H. Dicke, *Phys. Rev.* **93**, 99 (1954).
6. G. Birkl, et al., *Phys. Rev. Lett.* **75**, 2823 (1995).
7. M. Weidemüller, et al., *Phys. Rev. Lett.* **75**, 4583 (1995).
8. S. Slama, et al., *Phys. Rev. Lett.* **94**, 193901 (2005).
9. S. Slama, et al., *Phys. Rev. A* **73**, 023424 (2005).
10. B. T. Werner, *Science* **284**, 102 (1999).
11. S. Inouye, et al., *Science* **285**, 571 (1999).
12. M. Inouye, et al., *Science* **286**, 2309 (1999).
13. S. Slama, et al., *Phys. Rev. Lett.* **98**, 053603 (2007).
14. S. Slama, et al., *Phys. Rev. A* **75**, 063620 (2007).
15. R. Bonifacio, et al., *Nucl. Instrum. Methods Phys. Res. A* **341**, 360 (1994).
16. R. Bonifacio, et al., *Appl. Phys. B: Lasers Opt.* **60**, S233 (1995).
17. Y. Yoshikawa, et al., *Phys. Rev. Lett.* **94**, 083602 (2005).
18. W. Ketterle, et al., *Phys. Rev. Lett.* **86**, 4203 (2001).

19. M. G. Moore, et al., *Phys. Rev. Lett.* **86**, 4199 (2001).
20. D. Kruse, et al., *Phys. Rev. Lett.* **91**, 183601 (2003).
21. N. Piovella, et al., *Opt. Commun.* **187**, 165 (1997).
22. N. Piovella, et al., *Opt. Commun.* **194**, 167 (2001).
23. G. Robb, et al., *J. Opt. B: Quantum Semiclassical Opt.* **7**, 93 (2005).
24. S. Slama, Ph.D. thesis *Universität Tübingen, 2007* (http://www.uni-tuebingen.de/ub/elib/tobias.htm).
25. C. von Cube, et al., *Phys. Rev. Lett.* **93**, 083601 (2004).
26. M. G. Moore, et al., *Phys. Rev. A* **60**, 1491 (1999).
27. N. Piovella, et al., *Phys. Rev. A* **67**, 013817 (2003).
28. R. Bonifacio, et al., *Opt. Commun.* **137**, 276 (1997).
29. N. Piovella, et al., *Laser Physics* Vol. **17**, No. 2, pp. 174-179 (2006).
30. J. Klinner, et al., *Phys. Rev. Lett.* **96**, 023002 (2006).
31. D. Schneble, et al., *Science* **300**, 475 (2003).